THE JOURNAL OF BIOLOGICAL CHEMISTRY VOL. 289, NO. 15, pp. 10387–10398, April 11, 2014

The N-terminal Domain Tethers the Voltage-gated Calcium Channel β_{2e}-subunit to the Plasma Membrane via Electrostatic and Hydrophobic Interactions*

Received for publication, August 7, 2013, and in revised form, January 14, 2014 Published, JBC Papers in Press, February 11, 2014, DOI 10.1074/jbc.M113.507244

Erick Miranda-Laferte[‡], David Ewers[§], Raul E. Guzman[‡], Nadine Jordan[‡], Silke Schmidt[§], and Patricia Hidalgo[‡1]

From the [‡]Institute of Complex Systems 4, Zelluläre Biophysik (ICS-4), Forschungszentrum Jülich, 52425 Jülich and the [§]Institut für Neurophysiologie, Medizinische Hochschule Hannover, 30625 Hannover, Germany

Background: Membrane recruitment of the calcium channel β_{2e}-subunit remains elusive.
Results: Charge neutralization of β_{2e} N-terminal residues abolishes its lipid-binding and surface-targeting abilities and its slow inactivation-conferring phenotype.
Conclusion: The β_{2e}-subunit anchors to the membrane via electrostatic interactions likely involving an N-terminal in-plane α-helix and a tryptophan side-chain penetration.
Significance: A novel mechanism for β-subunit membrane-anchoring supporting slow inactivation is presented.

The β-subunit associates with the α_1 pore-forming subunit of high voltage-activated calcium channels and modulates several aspects of ion conduction. Four β-subunits are encoded by four different genes with multiple splice variants. Only two members of this family, β_{2a} and β_{2e}, associate with the plasma membrane in the absence of the α_1-subunit. Palmitoylation on a di-cysteine motif located at the N terminus of β_{2a} promotes membrane targeting and correlates with the unique ability of this protein to slow down inactivation. In contrast, the mechanism by which β_{2e} anchors to the plasma membrane remains elusive. Here, we identified an N-terminal segment in β_{2e} encompassing a cluster of positively charged residues, which is strictly required for membrane anchoring, and when transferred to the cytoplasmic β_{1b} isoform it confers membrane localization to the latter. In the presence of negatively charged phospholipid vesicles, this segment binds to acidic liposomes dependently on the ionic strength, and the intrinsic fluorescence emission maxima of its single tryptophan blue shifts considerably. Simultaneous substitution of more than two basic residues impairs membrane targeting. Coexpression of the fast inactivating R-type calcium channels with wild-type β_{2e}, but not with a β_{2e} membrane association-deficient mutant, slows down inactivation. We propose that a predicted α-helix within this domain orienting parallel to the membrane tethers the β_{2e}-subunit to the lipid bilayer via electrostatic interactions. Penetration of the tryptophan side chain into the lipidic core stabilizes the membrane-bound conformation. This constitutes a new mechanism for membrane anchoring among the β-subunit family that also sustains slowed inactivation.

The α_1-subunit ($Ca_V\alpha_1$) of HVA[2] calcium channels encompasses the ion conduction pathway, the voltage sensor, and the multiple intracellular domains that provide sites of interaction for regulatory proteins (1). One of these proteins is the β-subunit ($Ca_V\beta$) that binds to a highly conserved site among HVA channels and modulates several aspects of channel function, including surface expression and biophysical properties (2, 3). $Ca_V\beta$s are special members of the membrane-associated guanylate kinase family of proteins containing only two of the three canonical domains shared by this group as follows: an Src homology 3 (SH3) and a guanylate kinase domain (4–6). In contrast to these highly conserved domains, the linker region between them as well as the N- and C-terminal flanking segments (*HOOK*, *NT*, and *CT*, respectively, Fig. 1) vary in sequence and length among the four β-subunit isoforms (β_1 to β_4) identified until now. Each β subtype is encoded by a different gene that generates multiple splice variants giving rise to functionally different proteins. An extreme case occurs among the β_2 splice variants (β_{2a} to β_{2e}) that, despite their sequence similarity, have different subcellular localizations and even have opposing regulatory effects on calcium currents (7, 8). β_2 variants are between 604 and 655 amino acids long and they differ only in their most proximal N-terminal segment, hereafter referred to as NT_v (the subscript v stands for variable, Fig. 1). The subtypes 2a and 2e are the only members of the $Ca_V\beta$ family that are targeted to the plasma membrane in the absence of the α_1 pore-forming subunit, and when associated with it, they inhibit the voltage-dependent inactivation of the channel complex (7, 9, 10). Coexpression of the fast-inactivating R-type calcium channel with β_{2a} in *Xenopus laevis* oocytes or mamma-

* This work was supported by Deutsche Forschungsgemeinschaft Grant Hi 800/3-1 (to P. H.).
[1] To whom correspondence should be addressed: Institute of Complex Systems, Zelluläre Biophysik (ICS-4), Forschungszentrum Jülich, 52425 Jülich, Germany. E-mail: pa.hidalgo@fz-juelich.de.

[2] The abbreviations used are: HVA, high voltage-activated; SH3, Src homology 3 domain; NT_v, N-terminal variable segment; LUV, large unilamellar vesicles; SUV, small unilamellar vesicles; MC, Manders coefficient; PC, 1-palmitoyl-2-oleoyl-*sn*-glycero-phosphocholine; PS, 1-palmitoyl-2-oleoyl-*sn*-glycero-3-phospho-L-serine; AID, α interaction domain.

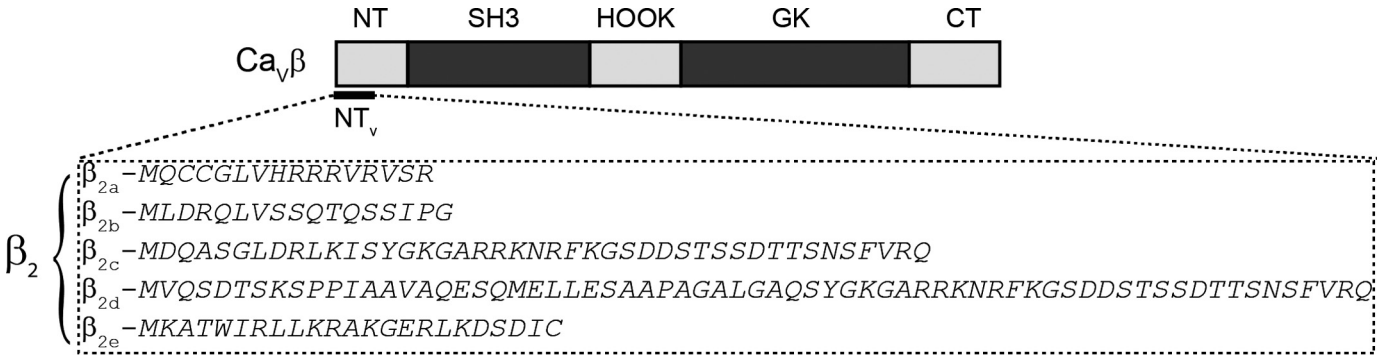

FIGURE 1. **Scheme of the domain organization of $Ca_V\beta$ and amino acid sequences of the N-terminal variable segments of β_2 splice variants.** The two highly conserved domains among the $Ca_V\beta$ family, SH3 and guanylate kinase (*GK*), shown in *dark gray*, are flanked by three nonconserved regions: N-terminal (*NT*), linker region joining the SH3 and GK domains (*HOOK*), and C-terminal (*CT*). The amino acid sequences corresponding to the variable segment (NT_V) among all β_2 splice variants (β_{2a} to β_{2e}) from rat are shown.

lian cell lines increases considerably the time needed for the current to return to 50% of its peak amplitude and shifts the steady-state inactivation curve toward more positive potentials as compared with channels composed of cytosolic, nonmembrane-associated β-isoforms (10–13). These unique modulatory properties of β_{2a} rely on two continuous N-terminal cysteine residues that undergo palmitoylation and target the protein to the plasma membrane (9, 14, 15). Substitution of these two residues disrupts membrane localization as well as the slow inactivation-conferring phenotype of β_{2a} (16). The prevalent view is that membrane anchoring restricts the free movement of the channel inactivation gate, preventing it from closing. Colecraft and co-workers (7) showed that $Ca_V1.2$ L-type calcium channels also inactivate more slowly in the presence of the two membrane-anchored β_2 variants as compared with their fully cytosolic distributed counterparts, β_{2b}, β_{2c}, and β_{2d}. In contrast to β_{2a}, the mechanism by which the β_{2e}-subunit is targeted to the plasma membrane remains to be elucidated. Here, we exchanged the variable N-terminal region between the β_{2e} and the β_{1b} isoform, which is distributed entirely in the cytoplasm, and we showed that this maneuver is sufficient to target the β_{1b} chimera to the plasma membrane. Moreover, the same N-terminal segment binds *in vitro* to negatively charged liposomes in an ionic strength-dependent manner. $\beta_{2e}NT_v$ includes seven positively charged residues and a net charge of +4 at physiological pH. We studied the role of these basic amino acids in membrane association and found that substitution of these residues by alanine inhibits the targeting of the protein to the plasma membrane and the *in vitro* interaction with anionic lipids. Coexpression of wild-type β_{2e} with the fast inactivating $Ca_V\alpha_1$ encoding the $Ca_V2.3$ R-type calcium channel results in channel complexes that inactivate significantly more slowly than $Ca_V2.3$ expressed with a β_{2e} mutant in which all positively charged residues within NT_v were replaced by alanine. Our results demonstrate that the positively charged N-terminal variable segment of β_{2e} is responsible for tethering the protein to the plasma membrane via electrostatic interactions and support the model suggesting that membrane anchoring underlies the slow inactivation-conferring phenotype.

EXPERIMENTAL PROCEDURES

cDNA Constructs—Full-length rat β_{2e} (UniProtKB accession number Q8VGC3-4) and rat β_{1b} (UniProtKB accession number P54283) cDNAs were subcloned into pcDNA 3.1 vector and fused at the C terminus to YFP (for confocal imaging) or monomeric red fluorescence protein (for electrophysiology) using standard overlapping PCR methods. β_{2e} mutants were generated by PCR using a common antisense and specific sense primers bearing the corresponding mutation. The chimeric $\beta_{2e}NT_v/\beta_{1b}$ was also generated using overlapping PCR methods by replacing residues 1–57 of β_{1b} with residues 1–23 of β_{2e}. The cDNAs encoding wild-type $\beta_{2e}NT_v$ (amino acids 1–23) or mutant versions were subcloned into PGEX 6P-1 vector using standard PCR methods to produce GST-$\beta_{2e}NT_v$ domain fusion constructs. YFP was fused to the N terminus of $Ca_V2.3$-coding region (UniProtKB accession number Q15878) using standard PCR methods and subcloned into pRcCMV vector.

Transfection of tsA201 Cells—For confocal microscopy, cells were grown on plastic μ-dishes (Ibidi) in Dulbecco's modified Eagle's medium supplemented with 10% fetal bovine serum and L-glutamine (2 mM) and incubated in a 5% CO_2-humidified atmosphere. Cells were transiently transfected using Lipofectamine 2000™ (Invitrogen) according to the manufacturer's instructions with the corresponding plasmids encoding the different β_{2e} derivatives. For whole-cell patch clamp recordings, cells were cotransfected with YFP-$Ca_V2.3$ and the corresponding β_{2e} fused to monomeric red fluorescence protein-encoding plasmids.

Confocal Microscopy and Colocalization Analysis—Confocal images were acquired 24–30 h after transfection on living cells using a 63× oil immersion objective on a Leica inverted confocal microscope. For colocalization analysis, prior to imaging the cells were stained with the plasma membrane marker CellMask™ (Invitrogen) according to the manufacturer's instructions. YFP fusion proteins were excited with a 514-nm laser, and emission was monitored at 520–550 nm, and the plasma membrane stain was excited at 633 nm and monitored at 640–700 nm. Quantification of the degree of colocalization between fluorescently labeled β-subunit and the plasma membrane marker was done by calculating the Manders coefficient (MC) using the JACoP plugin (17) embedded in ImageJ 1.44p software (National Institutes of Health, Bethesda) (18). At least five different fields of view (in total 100–200 transfected cells) for each β_{2e} derivative from at least two different transfections were analyzed. The Manders coefficient represents the fraction

of pixels in the YFP channel that overlaps with some signal in the CellMask™ (*red*) detection channel. For comparison of samples, a two-tailed Student's *t* test was used. Values are expressed as mean ± S.E.

Liposome Preparation—Phospholipid unilamellar vesicles were prepared by extrusion of multilamellar vesicles through 100-nm pore size polycarbonate filters using a handheld extruder (LiposoFast, Avestin, Inc). 1-Palmitoyl-2-oleoyl-*sn*-glycerophosphocholine (PC, Avanti 840034) either alone or combined with 1-palmitoyl-2-oleoyl-*sn*-glycero-3-phospho-L-serine (PS, Avanti 840034) in a 1:3 (PS/PC) molar ratio was dried under a stream of nitrogen. Any residual solvent was removed under vacuum. The resulting lipid film was rehydrated to reach a final concentration of 1 mM with a buffer containing 50 mM HEPES pH 7.5 supplemented with the indicated NaCl concentration and then subjected to three-to five freeze-thaw cycles using liquid nitrogen and a water bath at 37 °C. The lipid suspension was either extruded to obtain uniformly sized (about 100 nm diameter) large unilamellar vesicles (LUVs) for protein-liposome cosedimentation assays or sonicated at RT using a bath sonicator to obtain small unilamellar vesicles (SUVs) for tryptophan fluorescence studies (Morrissey Lab Protocols, University of Illinois) (19, 20).

Control PS/PC liposomes were prepared by adding 0.1% fluorescently labeled 7-nitro-2–1,3-benzoxadiazol-4-yl-PS (Avanti 810198). The fluorescence intensity was monitored using a microplate reader (FLUOstar Omega (BMG Labtec).

Protein-Liposome Cosedimentation Assays—Cosedimentation assays were performed as described previously (21). Briefly, 2.0 μg of protein were incubated with LUVs in 50 mM HEPES pH 7.5 buffer supplemented with the indicated NaCl concentration (total volume 100 μl) for 15 min at room temperature. Samples were ultracentrifuged at 150,000 × *g* for 40 min at 4 °C using a TLA 120.2 rotor (Beckman Instruments). Pellets were resuspended in the same volume as the supernatant, and equal volumes of each fraction from each sample were resolved by SDS-PAGE (12%). The quantification of proteins present in the different fractions was performed by densitometry of Coomassie Blue-stained gels using ImageJ software (18). The fraction of the protein bound to liposomes (protein-bound) was calculated from the quotient between the fraction of nonaggregated protein in the pellet and the pool of nonaggregated protein as shown in Equation 1,

$$\text{Protein-bound} = \frac{\text{Fraction nonaggregated protein in pellet}}{\text{Fraction nonaggregated protein}} = \frac{PP(Lip) - PP(\emptyset\ Lip)}{1 - PP(\emptyset\ Lip)} \quad \text{(Eq. 1)}$$

where *PP*(*Lip*) is the fraction of protein in the pellet in the presence of lipids, and *PP*(*Ø Lip*) is the fraction of protein in the pellet in the absence of liposomes (corresponding to the aggregated protein).

Tryptophan Fluorescence Measurements—Measurements were performed on a FluoroLog 3 spectrofluorometer (HORIBA Jobin Yvon) using 1–2 μM of a synthetic peptide (Eurogentec) containing the N-terminal region of β_{2e} (^{1}MKATWIRLLKRAKGERLKDSD^{21}) dissolved in different concentrations of SUVs in 50 mM HEPES pH 7.5 buffer supplemented with the indicated NaCl concentration. After combining the reagents in a 1-cm cuvette, the sample was mixed by pipetting and allowed to settle for ~5 min. Upon excitation of the samples at 280 nm, the emission spectrum was recorded in front face excitation mode from 290 to 440 or 300 to 440 nm. At each wavelength, the signal was integrated over 0.2 s. The bandwidth was 6–8 nm on the excitation side and 1–2.5 nm on the emission side to optimize the signal levels. Data analysis was performed using Origin (OriginLab) and SigmaPlot (Systat Software). To infer the wavelength of maximal emission, a log-normal distribution was fitted to the spectra (22). For the quantification of binding of vesicles to the peptide, it was assumed that the fluorescence emission results from a two-state equilibrium between unbound and bound peptide. It follows that every measured spectrum is a linear combination of two spectra. Accordingly, the fraction of peptide that is bound to lipids was determined by a deconvolution of the spectral data into the spectra resulting from experiments with 0 and 1.500 μM lipid concentration, corresponding to free and fully lipid-bound peptide, respectively (23). The resulting data were fitted by a Hill function.

Protein Purification—Wild-type β_{2e} and $\beta_{2e}NT_v$(7+ less), both fused to a hexahistidine tag, and the GST fusion proteins were expressed in bacteria and purified using affinity and size-exclusion chromatography as described previously (11).

Protein-Protein Binding Assays—The highly conserved β-binding site among all α_1 pore-forming subunits of high voltage gated calcium channels known the as α_1 interaction domain (AID) was fused to GST (GST-AID). Either 4 μg of GST-AID or of GST alone (in control experiments) was pre-coupled to glutathione beads (11). Coupled beads were then incubated with 4 μg of either β_{2e} or $\beta_{2e}NT_v$(7+ less) for 1 h at room temperature. After several washes, the bound proteins were eluted with SDS-loading buffer and resolved on SDS-PAGE. The gel was stained with Coomassie Blue.

Electrophysiological Recordings—Whole-cell patch clamp recordings were performed with an EPC-10 amplifier implemented with the PatchMaster software (HEKA, Elektronik). Borosilicate pipettes (Harvard Apparatus) with resistances of 0.9–2 megohms were pulled on a Sutter P-1000 puller (Harvard Apparatus) and fire-polished using a Narishige MF-830 microforge. Series resistance compensation was applied, resulting in less than 5-mV voltage error. The external recording solutions contained the following (in mM): 140 tetraethylammonium-$MeSO_3$, 10 $BaCl_2$, 10 HEPES buffer pH 7.3 adjusted with tetraethylammonium hydroxide although the internal solution contained 135 cesium-$MeSO_3$, 10 EGTA, 5 CsCl, 1 $MgCl_2$, 4 MgATP, 10 HEPES, and the pH was adjusted to 7.3 with CsOH. The data analysis was performed using a combination of FitMaster (HEKA), Origin (OriginLab), SigmaPlot (Systat Software), and Excel (Microsoft) software. All data are presented as mean ± S.E.

RESULTS

N Terminus of β_{2e} Is Responsible for Targeting the Protein to the Plasma Membrane—Because β_2 variants differ only in the most proximal amino acid sequence within the N-terminal region, it is likely that the differences in their subcellular loca-

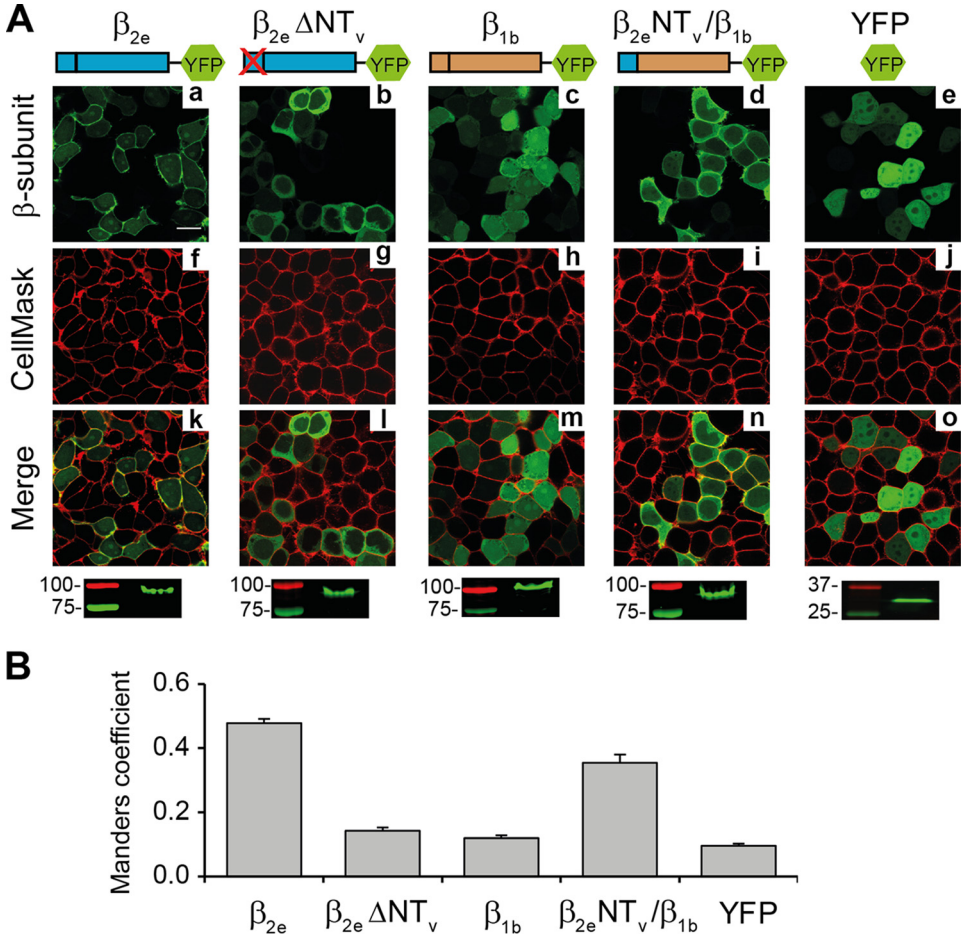

FIGURE 2. **The Variable N-terminal segment of the β_{2e}-subunit is responsible for targeting the protein to the plasma membrane.** *A*, confocal fluorescence images of tsA201 cells expressing the indicated protein constructs fused to YFP as follows: full-length β_{2e} (β_{2e}); β_{2e} lacking NT_V (β_{2e} ΔNT_V); full-length β_{1b} (β_{1b}); chimeric protein encompassing NT_V of β_{2e} in a β_{1b} background (β_{2e} NT_V/β_{1b}). YFP moiety alone was used as control protein. Prior to visualization, cells were stained with the red plasma membrane marker CellMask™. Images from β_{2e} fusion proteins, *green channel* (*panels a–e*); plasma membranes, *red channel* (*panels f–j*); and merge (*panels k–o*) are shown. *Scale bar*, 15 μm and is valid for all images. The *bottom panels* show crude lysates from cells expressing the indicated construct resolved by SDS-PAGE and visualized by fluorescence scanning. *Numbers* denote the molecular mass of standard proteins. The migration of the fusion constructs is consistent with their predicted molecular mass. *B*, bar plot of the colocalization analysis between β_{2e} derivatives and the plasma membrane marker according to Manders coefficient. Values are expressed as mean ± S.E.

tion are caused by signals within this part of the protein. To assess the impact of $\beta_{2e}NT_v$ on membrane anchoring, we deleted this segment (residues 2–23) from the rat β_{2e}. Wild-type β_{2e}, the deletion mutant, and the entire cytosolic β_{1b} isoform were expressed in tsA201 cells as YFP fusion proteins for confocal imaging analysis. Plasma membrane localization of the YFP fusion proteins was analyzed by staining the transfected cells with the CellMask™ plasma membrane marker and quantifying their degree of colocalization using the MC as described under "Experimental Procedures." For the plasma membrane-associated β_{2e}-YFP (7), we obtained an MC of 0.48 ± 0.01, for YFP alone, which distributes homogeneously within the cell, the value was 0.10 ± 0.01 (*t* test; $p < 0.01$, Fig. 2). After deletion of the NT_v segment, the degree of colocalization decreased significantly (MC = 0.14 ± 0.01, *t* test; $p < 0.01$, Fig. 2). We also exchanged the N-terminal variable regions between β_{2e} and the entire cytosolic β_{1b}-subunit to generate a chimeric protein encompassing $\beta_{2e}NT_v$ in the β_{1b} background ($\beta_{2e}NT_v/\beta_{1b}$). This maneuver increases MC from 0.12 ± 0.01 for β_{1b} to 0.35 ± 0.03 for the chimeric construct (*t* test; $p < 0.01$, Fig. 2*B*), a magnitude approaching that of wild-type β_{2e}. This indicates that substitution of the N-terminal segment of β_{1b} by $\beta_{2e}NT_v$ transfers to the former the capability to associate with the plasma membrane.

To exclude the possibility that the alterations in protein sorting were due to expression artifacts or degradation, crude homogenates from cells expressing the different fluorescent proteins were run on SDS-PAGE and visualized by fluorescence scanning (Fig. 2*A*, *bottom panels*). The results show that all YFP fusion proteins were expressed in their full length indicating that the changes observed in their subcellular location are associated with the absence or presence of $\beta_{2e}NT_v$. Together, these results demonstrate that $\beta_{2e}NT_v$ is the molecular determinant for targeting the protein to the plasma membrane.

The Variable N-terminal Segment of β_{2e} Associates in an Ionic Strength-dependent Manner with Phospholipid Vesicles—Peripheral membrane proteins commonly associate with the plasma membrane via covalent lipid modification of specific residues and/or via electrostatic interactions between positively charged amino acid residues and negatively charged phospholipids (24). Substitution of the single cysteine residue in $\beta_{2e}NT_v$ by alanine (β_{2e} C23A) does not impair the relocation

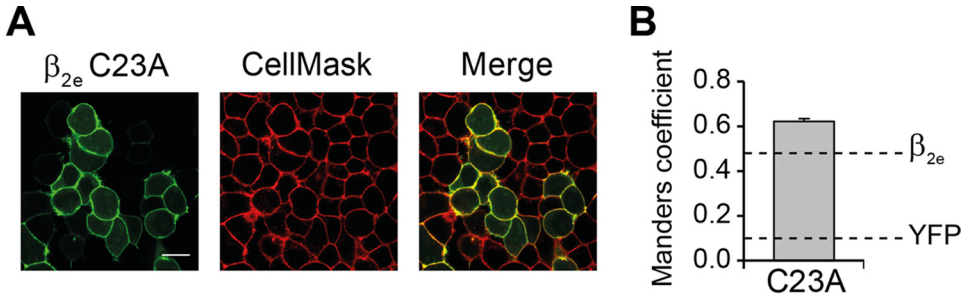

FIGURE 3. **Subcellular localization of β_{2e} C23A mutant protein.** *A*, confocal fluorescence images of tsA201 cells expressing β_{2e} C23A fused to YFP. Prior to visualization, cells were stained with the red plasma membrane marker CellMask™. Images from β_{2e} C23A fusion protein (*green channel*), plasma membranes (*red channel*), and merge are shown. *Scale bar,* 15 μm. *B,* bar plot of the colocalization analysis for β_{2e} C23A mutant. Values are expressed as mean ± S.E. *Dashed lines* correspond to the average values obtained for β_{2e} and YFP alone from Fig. 2*B*. The MC value for β_{2e} C23A was significantly different from that measured in cells expressing the wild-type protein (*t* test; $p < 0.05$).

of the protein to the plasma membrane (Fig. 3). The degree of colocalization between this mutant and the plasma membrane marker is slightly higher than the one estimated for the wild-type protein (MC = 0.62 ± 0.06, Fig. 3*B*). We conclude that palmitoylation is not responsible for the membrane association of this subunit, as is the case for β_{2a} (14). $\beta_{2e}NT_v$ contains no predictable additional protein modification sites such as prenylation or myristoylation but is enriched in positively charged residues. Therefore, we investigated the role of electrostatic interactions in the membrane association of β_{2e} using protein-liposome cosedimentation assays. $\beta_{2e}NT_v$ was fused to GST (GST-$\beta_{2e}NT_v$), expressed in bacteria, purified, and incubated at different ionic strengths with LUVs containing either negatively charged (PS/PC) or neutral (PC) phospholipids. After centrifugation, the supernatant and pellet fractions containing lipid-free and lipid-associated protein, respectively, were analyzed using SDS-PAGE (Fig. 4*A*). The presence of lipids in the supernatant and in the pellet fractions was confirmed in control experiments where a fluorescently labeled PS analog (7-nitro-2–1,3-benzoxadiazol-4-yl-PS) was added during the preparation of liposomes. The majority of the lipids was found in the pellet fraction at the different NaCl concentrations tested (99 ± 1, 96 ± 2, and 91 ± 4% in 50, 300, and 400 mM NaCl, respectively).

To discard the possibility that the protein observed in the pellet arises from an interaction between GST and the lipids, parallel experiments were performed in which GST-$\beta_{2e}NT_v$ was replaced by GST moiety alone. GST is virtually excluded from the pellet in all conditions after centrifugation (Fig. 4*A*).

A lower molecular band copurifies with GST-$\beta_{2e}NT_v$ and distributes almost evenly in the supernatant fraction (Fig. 4*A*). In Western blot analysis, this protein was recognized by an anti-GST antibody (Fig. 4*A*) indicating that it is a degradation product that may lack completely or partially the 23-amino acid residues of $\beta_{2e}NT_v$. Although unplanned, this protein provided an extra internal control for the assay.

A fraction of the GST-$\beta_{2e}NT_v$ is found in the pellet in the absence of phospholipids, indicating a degree of aggregation of the fusion protein arising from $\beta_{2e}NT_v$ moiety. Despite this, quantification of the protein bound to the liposomes demonstrates that at relatively low ionic strength (50 mM NaCl) a significantly higher amount of protein cosediments with negatively charged LUVs (PS/PC) than with neutral PC liposomes

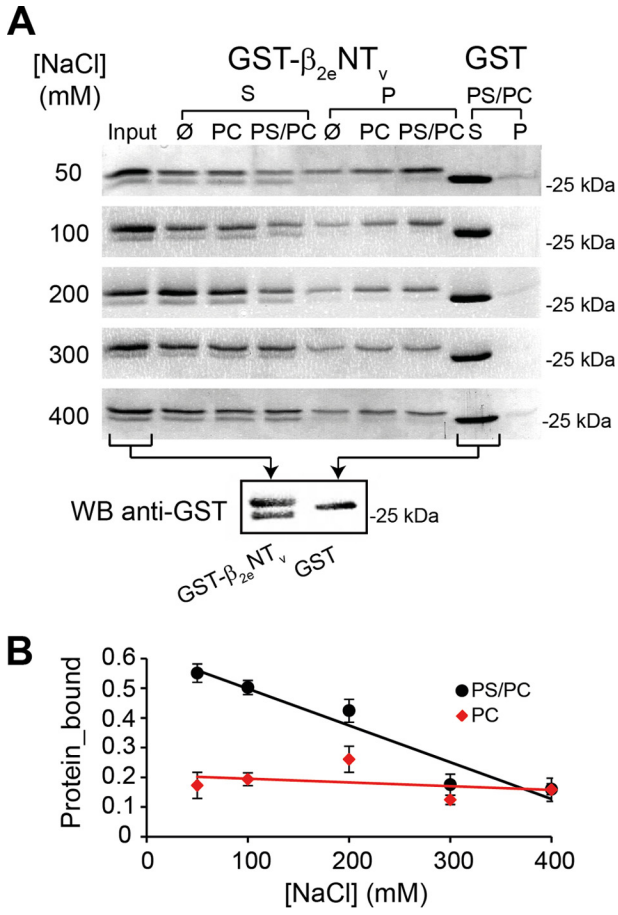

FIGURE 4. **Variable N-terminal segment of the β_{2e}-subunit binds to acidic liposomes in an ionic strength-dependent manner.** *A*, protein-liposome cosedimentation assays using $\beta_{2e}NT_v$ fused to GST (GST-$\beta_{2e}NT_v$). Representative SDS-PAGE gels from supernatant (*S*) and pellet (*P*) fractions after centrifugation of GST-$\beta_{2e}NT_v$ in assay buffer only (Ø indicates absence of liposomes) or preincubated with either neutral (PC) or negatively charged (PS/PC) liposomes at different NaCl concentrations from 50 to 400 mM. Controls assays using the GST moiety alone mixed with PS/PC liposomes were performed in parallel (*last two lanes*). A reference lane (*input*) that contains the total amount of protein used in each assay (2 μg) was included. Each assay was repeated at least three times. The *bottom panel* shows a Western blot (*WB*) analysis using an anti-GST antibody of the recombinant proteins used, GST-$\beta_{2e}NT_v$ and GST alone. *B*, plot of the fraction of GST-$\beta_{2e}NT_v$ bound to either PS/PC or PC liposomes at different NaCl concentrations. For details see under "Experimental Procedures." Values are expressed as mean ± S.E.

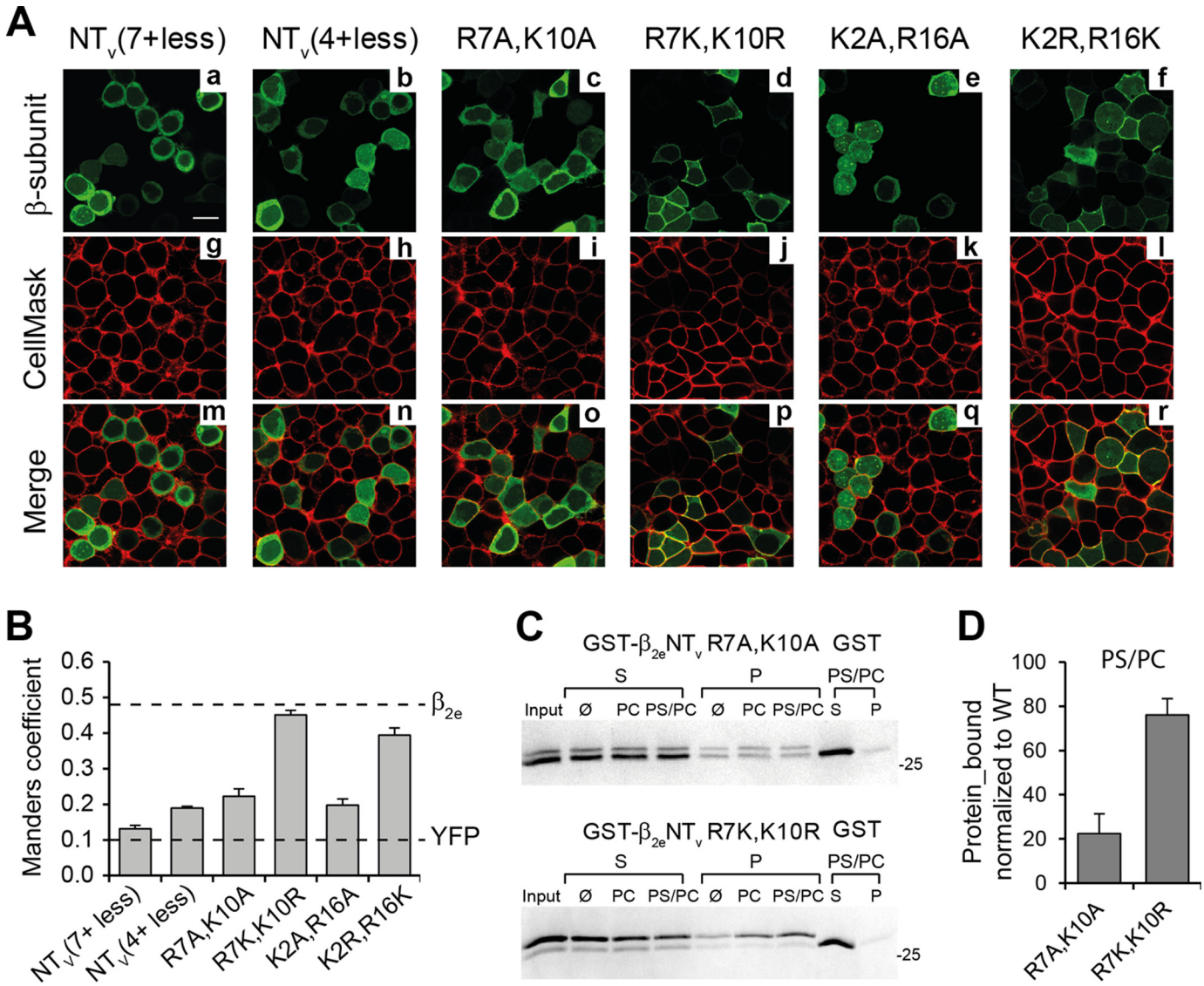

FIGURE 5. **Charge-neutralizing mutations of the basic residues within $\beta_{2e}NT_v$ impair the association of the protein with the plasma membrane.** *A,* confocal fluorescence images of tsA201 cells expressing β_{2e} mutants bearing the indicated simultaneous amino acid substitutions of lysine and arginine residues within NT_v as follows: NT_v(7+ less), seven lysine and arginine residues at NT_v were substituted by alanine; NT_v(4+ less), four basic residues were replaced with alanine (Arg^{11}, Lys^{13}, Arg^{16}, and Lys^{18}), and R7A,K10A, K2A,R16A, R7K,K10R, and K2R,R16K. β_{2e} mutant proteins (*panels a–f*), plasma membranes (*panels g–l*), and merge images (*panels m–r*) visualized as in Fig. 2*A*. *Scale bar,* 15 μm and is valid for all images. *B, bar plot* of the colocalization analysis for the mutant proteins shown in *A* done as in Fig. 2*B*. *Dashed lines* correspond to the average values obtained for β_{2e} and YFP alone from Fig. 2*B*. *C,* protein-liposome cosedimentation assays in 50 mM NaCl (as described in Fig. 4*A*) for $\beta_{2e}NT_v$ bearing the charge-neutralizing R7A,K10A (GST-$\beta_{2e}NT_v$ R7A,K10A, *top panel*) and the charge-conserving mutations at the same positions (GST-$\beta_{2e}NT_v$ R7K,K10R, *bottom panel*). *D*, plot of the fraction of protein bound to anionic liposomes (PS/PC) normalized to wild-type GST-$\beta_{2e}NT_v$ under the same salt conditions (50 mM NaCl). Values are expressed as mean ± S.E.

(Fig. 4*B*). Moreover, association of GST-$\beta_{2e}NT_v$ with PS/PC liposomes shows more acute dependence on the salt concentration (Fig. 4*B*). Increasing the ionic strength up 400 mM NaCl results in a persistent decrease in the quantity of GST-$\beta_{2e}NT_v$ found in the pellet with PS/PC liposomes that is not observed in the presence of PC liposomes. Altogether, these results indicate that electrostatic interactions play an important role in the binding of $\beta_{2e}NT_v$ to anionic liposomes.

Positively Charged Residues within $\beta_{2e}NT_v$ Are Required for Targeting the Protein to the Plasma Membrane—The binding of $\beta_{2e}NT_v$ to negatively charged phospholipid vesicles implies that positively charged residues within this segment are key players. To test this, we generated several β_{2e} constructs bearing simultaneous substitutions of lysine and arginine residues within $\beta_{2e}NT_v$, in which alanine replaced either all seven ($\beta_{2e}NT_v$(7+ less)), four ($\beta_{2e}NT_v$(4+ less)), or two basic residues at once (β_{2e} R7A,K10A and β_{2e}K2A,R16A). Quantification of the plasma membrane localization of these mutant proteins was done as in Fig. 2. Substitution of all seven positively charged residues decreased dramatically the degree of colocalization as compared with the wild-type protein (MC = 0.13 ± 0.01 for $\beta_{2e}NT_v$(7+ less), *t* test; $p < 0.01$, Fig. 5*B*). The MC value obtained for $\beta_{2e}NT_v$(7+ less) is comparable with the one estimated for YFP alone indicating a loss of surface membrane targeting. Neutralization of four or two basic residues also leads to a significant decrease in the plasma membrane localization of the protein (MC = 0.19 ± 0.01 for $\beta_{2e}NT_v$(4+ less), 0.22 ± 0.02 for β_{2e} R7A,K10A and 0.20 ± 0.02 for β_{2e}K2A,R16A, *t* test; $p <$

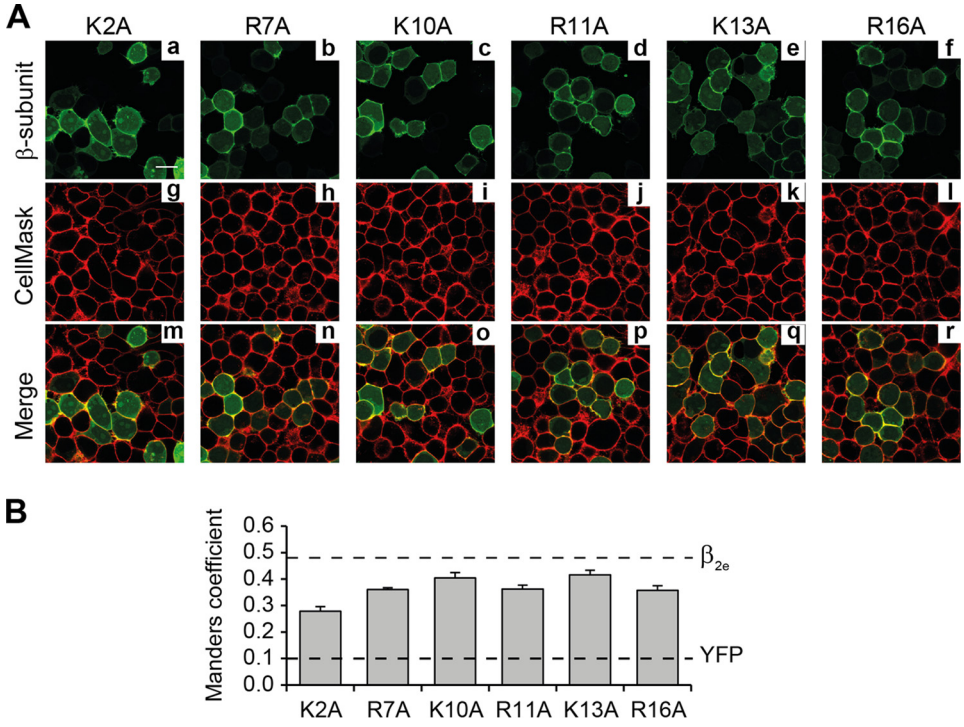

FIGURE 6. **Individual substitutions of positively charged residues within $\beta_{2e}NT_v$ differentially alter plasma membrane targeting.** *A*, confocal fluorescence images of tsA201 cells expressing the indicated β_{2e} mutations at single lysine or arginine residues within $\beta_{2e}NT_v$. β_{2e} single-point mutants (*panels a–f*), plasma membranes (*panels g–l*), and merged images (*panels m–r*) are visualized as in Fig. 2*A*. *Scale bar* represents 15 μm and is valid for all images. *B,* colocalization analysis and *dashed lines* as in Fig. 5*B*.

0.01, Fig. 5, *A* and *B*). However, the charge-conserving mutations of the double mutant proteins at the same amino acid positions (β_{2e} R7K,K10R and β_{2e} K2R,R16K, Fig. 5, *A* and *B*) preserve plasma membrane localization, demonstrating that the charge of the residue is the determinant factor in targeting the protein to the surface membrane.

We introduced the double mutations R7A,K10A and R7K, K10R into the GST-$\beta_{2e}NT_v$ fusion proteins (GST-$\beta_{2e}NT_v$ R7A,K10A and GST-$\beta_{2e}NT_v$ R7K,K10R, respectively) to investigate the correlation between surface membrane targeting and liposome binding. The charge neutralizing mutations significantly reduced the fraction of protein associated with negatively charged liposomes, whereas the ability of the charge conserving mutant to bind to PS/PC liposomes is preserved to a high extent as compared with wild-type $\beta_{2e}NT_v$ (Fig. 5, *C* and *D*). These results suggest that the loss of plasma membrane localization upon charge neutralization is mainly due to the impaired ability of the protein to establish electrostatic interactions with anionic phospholipids.

Single point mutations of all arginine or lysine residues within $\beta_{2e}NT_v$ to alanine moderately decrease the degree of colocalization with the plasma membrane marker compared with the WT protein (Fig. 6, *A* and *B*). The values of MC ranged between 0.36 ± 0.01 and 0.42 ± 0.02 for all proteins bearing a single residue mutation except for K2A mutant with an MC equal to 0.28 ± 0.02 (Fig. 6*B*). This suggests that Lys^2 is involved in a more intimate protein-membrane interaction.

Fluorescence Emission Maxima of the Trp^5 Blue Shifts in the Presence of Anionic Liposomes Indicating Penetration of This Residue into the Lipid Bilayer—Tryptophan residues in peripheral membrane proteins are commonly found in association with the membrane's hydrophobic core (25). We took advantage of the presence of a single tryptophan residue at position 5 (Trp^5) within $\beta_{2e}NT_v$ to study the association of this segment with lipids using intrinsic fluorescence measurements. At first, we substituted this residue by alanine in β_{2e}-YFP and found that this mutation results in a significant decrease in the degree of colocalization with the plasma membrane marker (MC = 0.16 ± 0.01) compared with WT (Fig. 7, *A* and *B*). However, the binding of $\beta_{2e}NT_v$ W5A to negatively charged liposomes under low salt conditions (50 mM NaCl) is only slightly diminished as compared with wild-type $\beta_{2e}NT_v$, although association with neutral liposomes is significantly impaired (Fig. 7, *C* and *D*). This indicates that Trp^5 may indeed contribute directly to lipid binding through hydrophobic interactions, which will be more relevant at the relatively higher ionic strength of the cellular environment.

At a low salt concentration, incubation of a synthetic peptide corresponding to $\beta_{2e}NT_v$ (residues 1–21) with increasing concentrations of negatively charged PS/PC SUVs induced a pronounced blue shift in Trp^5 fluorescence emission maximum with a concomitant increase in the fluorescence intensity (Fig. 7*E*). The observed shift in emission maximum from 346 nm in the absence of vesicles to 323 nm in the presence of saturating PS/PC concentrations (Fig. 7*F*) indicates that this residue changes from an aqueous into an essentially hydrophobic environment (*e.g.* the hydrocarbon core of the membrane) (see also "Discussion") (26). The fit of a Hill function to the lipid concentration dependence of the fraction of bound peptide at low ionic strength yields a K_D of 182 ± 34 μM (Fig. 7*G*).

At higher ionic strength (400 mM NaCl), full binding was not reached with the employed lipid concentrations (Fig. 7*F*) indi-

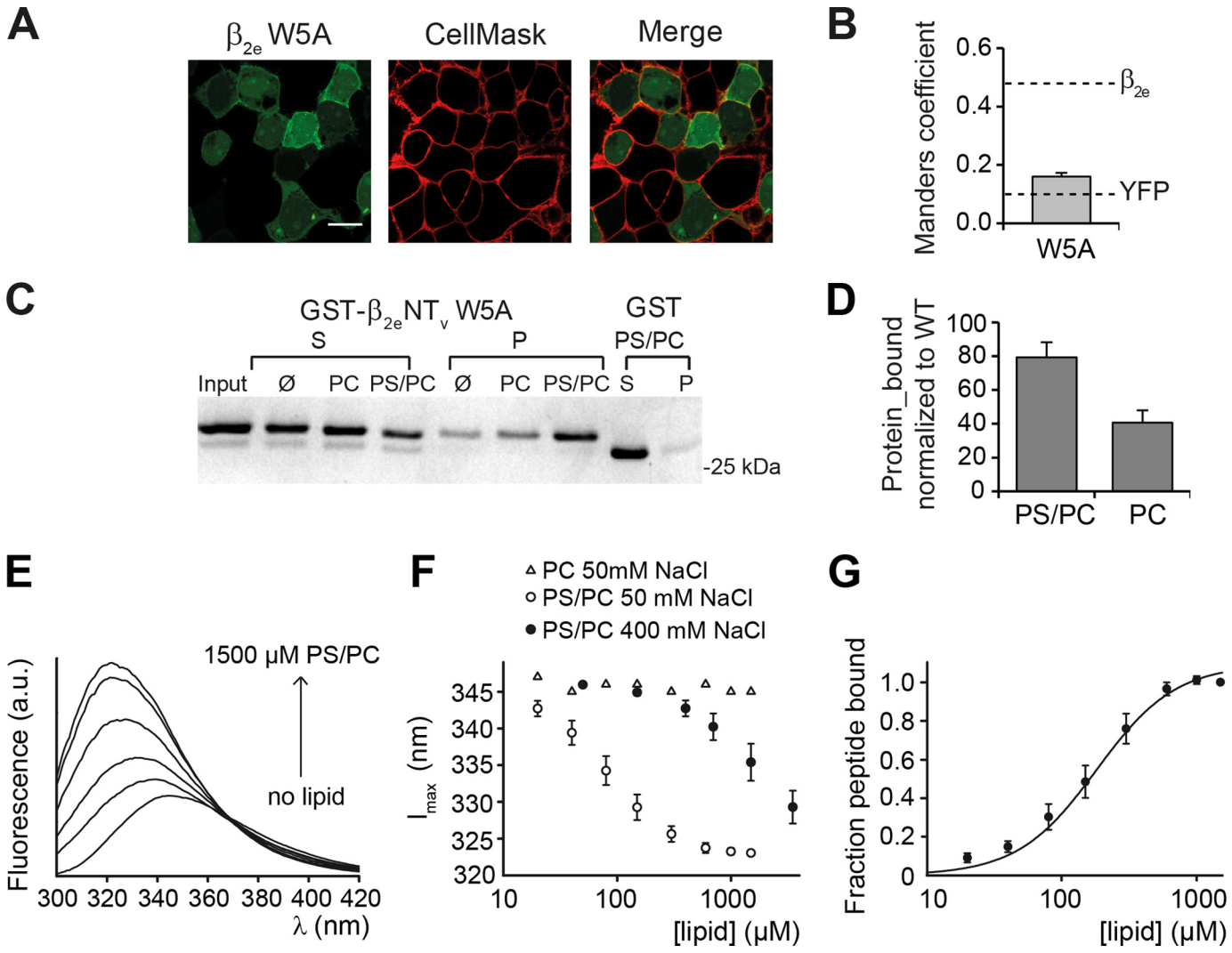

FIGURE 7. **Hydrophobic interactions mediated by the single tryptophan residue within $\beta_{2e}NT_v$ contribute to the plasma membrane targeting of the β_{2e} subunit.** *A,* confocal fluorescence images of tsA201 cells expressing β_{2e} W5A fused to YFP and stained with the CellMask™ plasma membrane marker, visualized using the *green* and *red channel*, respectively. *Scale bar,* 15 μm. *B,* colocalization analysis for β_{2e} W5A, and *dashed lines* are as in Fig. 3*B*. *C,* representative protein-liposome cosedimentation assay of GST-$\beta_{2e}NT_v$ W5A. *D,* plot of the fraction of protein bound to anionic (PS/PC) and neutral (PC) liposomes normalized to wild-type GST-$\beta_{2e}NT_v$ under the same salt conditions (50 mM NaCl). Values are expressed as mean ± S.E. *E,* representative emission spectra of $\beta_{2e}NT_v$ peptide (residues 1–21) after excitation with 280 nm in the presence of 50 mM NaCl and different concentrations of PC/PS SUVs. The lipid concentrations were (in order of increasing peak intensity, in μM) 0, 80, 150, 300, 600, and 1500. *F,* plot of emission maxima of spectra as shown in *E* against the lipid concentrations of PC/PS SUVs at 50 and 400 mM NaCl, as well as PC SUV at 50 mM NaCl. *G,* plot of the fraction of bound peptide (for details see under "Experimental Procedures") against the lipid concentration of PC/PS SUVs at 50 mM NaCl. The *line* represents the fit of a Hill equation to the data, resulting in $K_D = 182 \pm 34$ μM and $n_H = 1.5 \pm 0.1$. Values are expressed as mean ± S.E.

cating a decrease of the binding affinity. This finding is consis$_{2e}NT_v$ to PS/PC liposomes observed in cosedimentation assays (see Fig. 4). In the presence of neutral PC vesicles, virtually no changes in the intrinsic Trp^5 fluorescence were monitored at all salt concentrations tested (Fig. 7*F*). In contrast, we observed a small fraction of the GST-$\beta_{2e}NT_v$ cosedimenting with PC vesicles (Fig. 4). Although the cause of this difference is unclear, it is worth noting that fluorescence measurements were performed with SUVs, rather than LUVs, to minimize differential light-scattering effects (19). Altogether these results indicate that Trp^5 penetrates into the plasma membrane when electrostatic interactions between the positively charged residues and the anionic lipids are allowed.

Plasma Membrane Anchoring of β_{2e} Regulates the Rate of Inactivation of R-type Calcium Channels—Coexpression of $Ca_V2.3$ with the membrane-anchored β_{2a} in tsA201 cells and *Xenopus* oocytes induces a dramatic increase in the time needed for the current to return to 50% of its peak amplitude (hereafter referred to as $t_{0.5}$) and shifts the steady-state inactivation curve toward more depolarizing voltages with respect to the $Ca_V2.3$ coexpressed with cytosolic β-isoforms (β_{1b}, β_3, and β_4) (10–13). Here, we compared the effects of the wild-type β_{2e}-subunit and the membrane association-deficient mutant containing no basic residues within $\beta_{2e}NT_v$ ($\beta_{2e}NT_v$(7+ less), see Fig. 5, *A* and *B*) on $Ca_V2.3$ channel complexes expressed in tsA201 cells.

We tested whether substitution of all positively charged residues in $\beta_{2e}NT_v$ interferes with the ability of the protein to bind to the α_1-subunit. For this purpose, the highly conserved binding site in all α_1-subunits of HVA, referred as to AID (27), was fused to GST (GST-AID) and used as bait protein in a standard *in vitro* binding assay. Either wild-type β_{2e} or the $\beta_{2e}NT_v$(7+ less) were added as prey. Control binding reactions

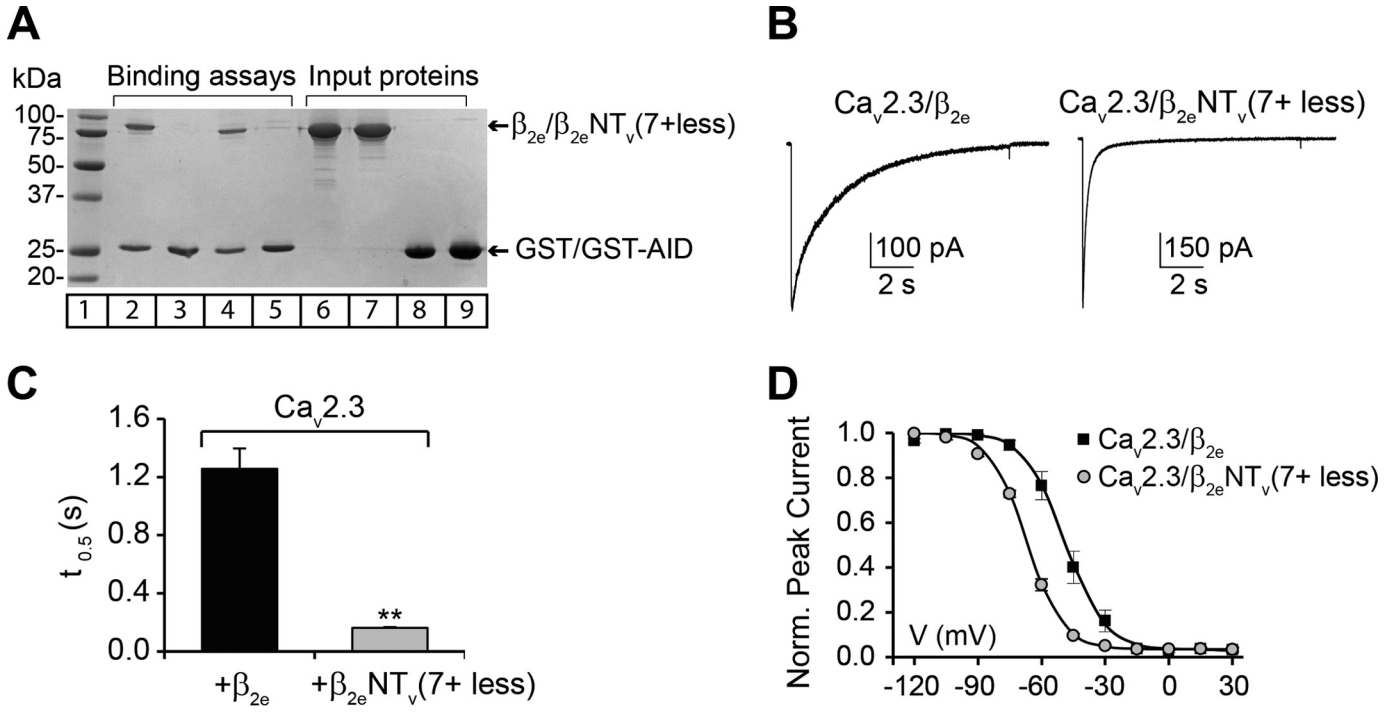

FIGURE 8. **Membrane association of the β_{2e}-subunit modulates the voltage-dependent inactivation of the R-type calcium channels.** *A,* binding assay of wild-type β_{2e} and $\beta_{2e}NT_v(7+$ less) membrane association-deficient mutant to the highly conserved α_1 interaction domain (AID). Either GST moiety alone or AID site fused to GST (GST-AID) were pre-coupled to glutathione-agarose beads and incubated with either wild-type β_{2e} or $\beta_{2e}NT_v(7+$ less) proteins. After several washes, the bound proteins were eluted and resolved on SDS-PAGE. *Lane 1*, molecular mass in kDa; *lane 2*, binding of wild-type β_{2e} to GST-AID; *lane 3*, binding of wild-type β_{2e} to GST; *lane 4*, binding of $\beta_{2e}NT_v(7+$ less) to GST-AID; *lane 5*, binding of $\beta_{2e}NT_v(7+$ less) to GST; *lanes 6-9*, inputs proteins. *B,* representative current traces from tsA201 cells coexpressing the R-type $Ca_V2.3$ α_1-subunit of voltage-activated calcium channels either with wild-type β_{2e} or β_2 $NT_v(7+$ less). Currents were elicited during a 10-s pulse to 0 mV from a holding potential of −90 mV. *C,* average $t_{0.5}$ for $Ca_V2.3/\beta_{2e}$ and $Ca_V2.3/\beta_{2e}NT_v(7+$ less) channel complexes. $t_{0.5}$ significantly decreases from 1.26 ± 0.14 s ($n = 6$) for $Ca_V2.3/\beta_{2e}$ to 0.16 ± 0.01 s ($n = 6$) for $Ca_V2.3/\beta_{2e}NT_v(7+$ less) channel complexes (*t* test; $p <$ 0.01). *D,* average steady-state inactivation curves from cells expressing the indicated channel subunit combinations. Inactivation was determined after a 10-s pre-pulse ranging from −120 to +30 mV in 15-mV increments from a holding potential of −90 mV followed by a short deactivation pulse to −90 mV and a 5-s test pulse at 0 mV. The interval between sweeps was of 60 s. *Continuous lines* correspond to the Boltzmann distribution that best fit the experimental data for the indicated channel complex. Values are expressed as mean ± S.E. $V_{0.5}$ significantly varies from −49.0 ± 3.1 mV ($n = 6$) for $Ca_V2.3$-β_{2e} to −67.0 ± 0.8 mV ($n =$ 6) for $Ca_V2.3$-$\beta_{2e}NT_v(7+$ less) channel complexes (*t* test; $p < 0.01$).

were performed in parallel using GST alone as bait. Both wild-type β_{2e} and the mutant protein bind to the GST-AID to a comparable extent (Fig. 8*A*).

Coexpression of $Ca_V2.3$ with the nonmembrane-associated $\beta_{2e}NT_v(7+$ less) mutant leads to an 8-fold decrease in $t_{0.5}$ at 0 mV as compared with $Ca_V2.3$ coexpressed with wild-type β_{2e} (Fig. 8, *B* and *C*). Moreover, the steady-state inactivation curve from cells expressing $Ca_V2.3$ and $\beta_{2e}NT_v(7+$ less) complexes is shifted to more negative potentials with respect to cells transfected with $Ca_V2.3$ and β_{2e} (Fig. 8*D*). Half-inactivation voltages ($V_{0.5}$) obtained from the fit to a Boltzmann distribution for $Ca_V2.3$ coexpressed with β_{2e} WT and mutant were similar to those previously reported for membrane-anchored β_{2a} and the cytosolic β_{1b}, respectively (12).

These results imply that different mechanisms of β-subunit membrane association lead to a functional analogy in the inhibition of the voltage dependence of inactivation.

DISCUSSION

Proteins use diverse mechanisms to associate with lipid membranes, including electrostatic interactions between protein segments enriched in positively charged amino acid residues and anionic lipids as well as hydrophobic interactions between the membrane lipids and nonpolar regions of the protein and/or covalently attached lipid anchors (24). Here, we identified a short domain located at the N-terminal region of β_{2e} that is responsible for tethering the protein to the plasma membrane. This domain consists of several positively charged residues distributed along 23 amino acids and hydrophobic residues intercalated between them. A consensus secondary structure prediction program that integrates several methods based on different principles (28) calculated a helical structure within residues 2–13. Most notably, within this putative helix a short in-plane membrane anchor segment was predicted (Fig. 9*A*) (29). This region is highly conserved across highly divergent species suggesting a conserved structure-function (Fig. 9*A*). Alanine scanning mutagenesis revealed that Lys^2 has a stronger effect on membrane affinity than the other residues (see Fig. 6). Lys^2 maps to the same side of a helical wheel plot together with the nonpolar Trp^5 and Leu^9 residues (Fig. 9*B*). The significant blue shift of the fluorescence emission of Trp^5 upon addition of negatively charged lipids indicates that this residue moves to a highly hydrophobic environment that is not likely to be provided by structural rearrangement of this short peptide bearing a net charge of +4. The direction and magnitude of the changes in the emission maxima of Trp^5 in the presence of anionic phospholipids are consistent with a relatively deep membrane penetration of this residue. Fluorescence studies on model peptides

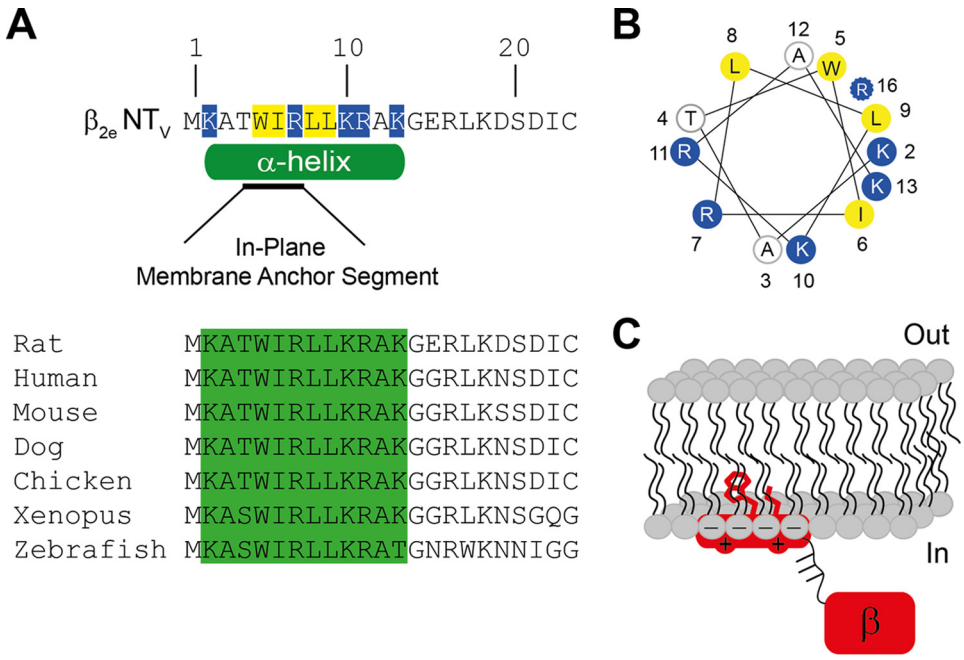

FIGURE 9. **Model depicting the association of the β_{2e}-subunit with the plasma membrane.** *A,* amino acid sequence and predicted secondary structure for the β_{2e} N-terminal variable region (β_{2e} *NT*$_V$). The positively charged and the nonpolar residues within β_{2e}NT$_V$ are highlighted in *blue* and *yellow*, respectively. The *green cylinder* below the sequence delimits the predicted α-helix (residues 2–13) according to the consensus secondary prediction results (NPS@Web server) (28). Within the helix an in-plane membrane anchor segment (residues 4–7) is predicted (*black line*) (29). The *lower panel* shows the amino acid alignment of β_{2e}NT$_V$ segment from (in *parenthesis*, UniProtKB accession numbers) rat (Q8VGC3), human (Q08289), mouse (Q8CC27), dog (E2RCN6), chicken (E1BZF6), *Xenopus* (F7EDB7), and zebrafish (B2XY77). *B,* helical wheel diagram of the predicted consensus helix within β_{2e}NT$_V$ extending from residues 2 to 13 (Helical Wheel Applet, University of Virginia). The potential location of Arg^{16} considering a longer helix is also shown (37). The relatively critical residues deduced from alanine scanning mutagenesis, Lys^2, Trp^5 together with Leu^9 (data not shown) lie on one side of the helix. *C,* proposed model to explain membrane anchoring of β_{2e}. The β_{2e}-subunit includes a helical membrane anchor site in its N-terminal region that associates *in plane* with the membrane via electrostatic interactions between its positively charged residues and the phospholipids headgroups. After the electrostatic recruitment of the protein to the plasma membrane, the bound conformation is stabilized by a relatively deep penetration of hydrophobic residues, including the aromatic side chain of Trp^5 and the aliphatic chain of Leu^9 into the lipid core. We suggest that the predicted phosphorylation sites (36), represented as *lines*, in the flexible segment joining the NT$_V$ helix and the core of the protein (labeled β) may induce dissociation of the protein from the plasma membrane, providing additional regulatory input for calcium entry through voltage-gated calcium channels.

assign an average distance of 7 Å from the lipid bilayer center to a Trp emission fluorescence wavelength maximum comparable with the one we observed with the β_{2e}NT$_V$ peptide at the highest lipid concentration (323 nm, Fig. 7, *E* and *F*) (30). Considering the width of a monolayer as 15 Å, this would imply that the Trp^5 penetrates about 8 Å into the plasma membrane beyond the lipid head groups and, consequently, that the putative in-plane helix is in close contact or interweaved with the headgroups (Fig. 9*C*). Aside from strengthening the association with the plasma membrane, the Trp^5 may be important for the intracellular trafficking of the protein, for example by promoting binding to intracellular membrane vesicles. This would explain why the protein bearing an alanine at that position binds to anionic lipids but is not found at the cell surface. Mutation of Leu^9 into alanine also results in a loss of plasma membrane targeting (data not shown), reinforcing the possibility that hydrophobic interactions may be important under physiological conditions for associating the protein with the plasma membrane. Our data are consistent with a mechanism by which β_{2e} anchors to the plasma membrane via an N-terminal helix that orients parallel to the plane of the bilayer (in-plane membrane association) and inserts relatively deeply into the headgroups (Fig. 9*C*). Association with the plasma membrane would take place in two steps as follows: first, the protein is recruited to the cell surface via electrostatic interactions with its positively charged residues, and second, the membrane-bound conformation is stabilized by the penetration of hydrophobic residues (*i.e.* Trp^5 and Leu^9) into the lipidic core. Although we cannot evaluate the precise contribution of electrostatic and hydrophobic interactions to the binding of β_{2e} to the plasma membrane *in vivo*, our experiments show that hydrophobic interactions become more relevant in the relatively higher ionic strength of the cellular environment.

The interaction with lipids can alter the subcellular localization, conformation, and activity of proteins. An example is β_{2a}, which switches from a fast to a slow inactivation-conferring phenotype upon palmitoylation and membrane association. Here, we demonstrated that β_{2e} is not an exception; when associated with the plasma membrane, β_{2e} displays very different channel modulatory activity compared with the membrane anchor-deficient mutant. The fact that both β_{2a} and β_{2e} inhibit voltage-dependent inactivation of Ca$_V$2.3 channels, although they associate differently with lipids, supports the model suggesting that membrane anchoring is sufficient to slow down channel inactivation by restricting the movement of the inactivation gate (31).

The dynamic nature of β_{2a} palmitoylation provides a further control mechanism regulating *in vivo* calcium influx through voltage-gated calcium channels (15). However, it remains unknown whether or not the association of β_{2e} with the cell membrane is subject to regulation *in vivo*. In fluorescence confocal images of cells expressing β_{2e}, the protein distributes mainly in the surface membrane, but a slight dif-

fuse fluorescence is visible within the cell, arguing in favor of a regulated membrane targeting (32). Although additional experiments will be required to test this hypothesis, we speculate that the phosphorylation state of the β_{2e} N-terminal domain may be particularly important for controlling the association of this subunit with the plasma membrane as has been suggested for other proteins (32, 33). Phosphorylation of $Ca_V\beta$ subunits that play a role in channel regulation has been described (34, 35). The N-terminal region of β_{2e} contains several potential phosphorylation sites downstream of the membrane anchor segment identified in this study. Prediction programs reveal a phosphorylation hot spot within a very short protein segment encompassing residues 29–39 (36). Phosphorylation of these sites would decrease the positive charge density of $\beta_{2e}NT_v$ and, consequently, weaken its interaction with membrane lipids.

In summary, in addition to providing a mechanism by which β_{2e} anchors to the plasma membrane, our study suggests a structure for the N-terminal region of the protein for which no data are available. The high resolution structure of three β isoforms (β_2, β_3, and β_4) has been solved, but these do not provide structural data for the variable regions outside the SH3-guanylate kinase domains.

This is the first β-subunit described that associates with the plasma membrane via electrostatic interactions. The fact that single point mutations within this domain appear to alter the protein membrane affinity makes it feasible to use this protein as a model to correlate membrane binding affinities to the degree of inhibition of voltage-dependent inactivation conferred by membrane-anchored β-subunits.

Acknowledgments—We thank Drs. Christoph Fahlke, Ingo Weyand, and Juan Garcia for insightful discussion.

REFERENCES

1. Catterall, W. A. (2011) Voltage-gated calcium channels. *Cold Spring Harbor Perspect. Biol.* **3,** a003947
2. Dolphin, A. C. (2003) β subunits of voltage-gated calcium channels. *J. Bioenerg. Biomembr.* **35,** 599–620
3. Hidalgo, P., and Neely, A. (2007) Multiplicity of protein interactions and functions of the voltage-gated calcium channel β-subunit. *Cell Calcium* **42,** 389–396
4. Chen, Y. H., Li, M. H., Zhang, Y., He, L. L., Yamada, Y., Fitzmaurice, A., Shen, Y., Zhang, H., Tong, L., and Yang, J. (2004) Structural basis of the α_1-β subunit interaction of voltage-gated Ca^{2+} channels. *Nature* **429,** 675–680
5. Opatowsky, Y., Chen, C. C., Campbell, K. P., and Hirsch, J. A. (2004) Structural analysis of the voltage-dependent calcium channel β-subunit functional core and its complex with the α_1-interaction domain. *Neuron* **42,** 387–399
6. Van Petegem, F., Clark, K. A., Chatelain, F. C., and Minor, D. L., Jr. (2004) Structure of a complex between a voltage-gated calcium channel β-subunit and an α-subunit domain. *Nature* **429,** 671–675
7. Takahashi, S. X., Mittman, S., and Colecraft, H. M. (2003) Distinctive modulatory effects of five human auxiliary β_2 subunit splice variants on L-type calcium channel gating. *Biophys. J.* **84,** 3007–3021
8. Link, S., Meissner, M., Held, B., Beck, A., Weissgerber, P., Freichel, M., and Flockerzi, V. (2009) Diversity and developmental expression of L-type calcium channel β_2 proteins and their influence on calcium current in murine heart. *J. Biol. Chem.* **284,** 30129–30137
9. Chien, A. J., Gao, T., Perez-Reyes, E., and Hosey, M. M. (1998) Membrane targeting of L-type calcium channels. Role of palmitoylation in the subcellular localization of the β_{2a} subunit. *J. Biol. Chem.* **273,** 23590–23597
10. Olcese, R., Qin, N., Schneider, T., Neely, A., Wei, X., Stefani, E., and Birnbaumer, L. (1994) The amino termini of calcium channel β-subunits set rates of inactivation independently of their effect on activation. *Neuron* **13,** 1433–1438
11. Hidalgo, P., Gonzalez-Gutierrez, G., Garcia-Olivares, J., and Neely, A. (2006) The α_1-β subunit interaction that modulates calcium channel activity is reversible and requires a competent α-interaction domain. *J. Biol. Chem.* **281,** 24104–24110
12. Jones, L. P., Wei, S. K., and Yue, D. T. (1998) Mechanism of auxiliary subunit modulation of neuronal α_{1E} calcium channels. *J. Gen. Physiol.* **112,** 125–143
13. Yasuda, T., Chen, L., Barr, W., McRory, J. E., Lewis, R. J., Adams, D. J., and Zamponi, G. W. (2004) Auxiliary subunit regulation of HVA calcium channels expressed in mammalian cells. *Eur. J. Neurosci.* **20,** 1–13
14. Chien, A. J., Carr, K. M., Shirokov, R. E., Rios, E., and Hosey, M. M. (1996) Identification of palmitoylation sites within the L-type calcium channel β_{2a} subunit and effects on channel function. *J. Biol. Chem.* **271,** 26465–26468
15. Qin, N., Platano, D., Olcese, R., Costantin, J. L., Stefani, E., and Birnbaumer, L. (1998) Unique regulatory properties of the type 2a Ca^{2+} channel β-subunit caused by palmitoylation. *Proc. Natl. Acad. Sci. U.S.A.* **95,** 4690–4695
16. Gonzalez-Gutierrez, G., Miranda-Laferte, E., Nothmann, D., Schmidt, S., Neely, A., and Hidalgo, P. (2008) The guanylate kinase domain of the β-subunit of voltage-gated calcium channels suffices to modulate gating. *Proc. Natl. Acad. Sci. U.S.A.* **105,** 14198–14203
17. Bolte, S., and Cordelières, F. P. (2006) A guided tour into subcellular colocalization analysis in light microscopy. *J. Microsc.* **224,** 213–232
18. Schneider, C. A., Rasband, W. S., and Eliceiri, K. W. (2012) NIH Image to ImageJ: 25 years of image analysis. *Nat. Methods* **9,** 671–675
19. Mao, D., and Wallace, B. A. (1984) Differential light scattering and absorption flattening optical effects are minimal in the circular dichroism spectra of small unilamellar vesicles. *Biochemistry* **23,** 2667–2673
20. Mui, B., Chow, L., and Hope, M. J. (2003) Extrusion technique to generate liposomes of defined size. *Methods Enzymol.* **367,** 3–14
21. Hui, E., Bai, J., and Chapman, E. R. (2006) Ca^{2+}-triggered simultaneous membrane penetration of the tandem C2-domains of synaptotagmin I. *Biophys. J.* **91,** 1767–1777
22. Burstein, E. A., and Emelyanenko, V. I. (1996) Log-normal description of fluorescence spectra of organic fluorophores. *Photochem. Photobiol.* **64,** 316–320
23. Keller, S., Böthe, M., Bienert, M., Dathe, M., and Blume, A. (2007) A simple fluorescence-spectroscopic membrane translocation assay. *Chembiochem* **8,** 546–552
24. Khandelia, H., Ipsen, J. H., and Mouritsen, O. G. (2008) The impact of peptides on lipid membranes. *Biochim. Biophys. Acta* **1778,** 1528–1536
25. Lomize, A. L., Pogozheva, I. D., Lomize, M. A., and Mosberg, H. I. (2007) The role of hydrophobic interactions in positioning of peripheral proteins in membranes. *BMC Struct. Biol.* **7,** 44
26. Reshetnyak, Y. K., Koshevnik, Y., and Burstein, E. A. (2001) Decomposition of protein tryptophan fluorescence spectra into log-normal components. III. Correlation between fluorescence and microenvironment parameters of individual tryptophan residues. *Biophys. J.* **81,** 1735–1758
27. Pragnell, M., De Waard, M., Mori, Y., Tanabe, T., Snutch, T. P., and Campbell, K. P. (1994) Calcium channel β-subunit binds to a conserved motif in the I-II cytoplasmic linker of the α_1-subunit. *Nature* **368,** 67–70
28. Combet, C., Blanchet, C., Geourjon, C., and Deléage, G. (2000) NPS@: network protein sequence analysis. *Trends Biochem. Sci.* **25,** 147–150
29. Sapay, N., Guermeur, Y., and Deléage, G. (2006) Prediction of amphipathic in-plane membrane anchors in monotopic proteins using a SVM classifier. *BMC Bioinformatics* **7,** 255
30. Chung, L. A., Lear, J. D., and DeGrado, W. F. (1992) Fluorescence studies of the secondary structure and orientation of a model ion channel peptide in phospholipid vesicles. *Biochemistry* **31,** 6608–6616
31. Stotz, S. C., Jarvis, S. E., and Zamponi, G. W. (2004) Functional roles of cytoplasmic loops and pore lining transmembrane helices in the voltage-

dependent inactivation of HVA calcium channels. *J. Physiol.* **554,** 263–273
32. Cornell, R. B., and Taneva, S. G. (2006) Amphipathic helices as mediators of the membrane interaction of amphitropic proteins, and as modulators of bilayer physical properties. *Curr. Protein Pept. Sci.* **7,** 539–552
33. Cho, W., and Stahelin, R. V. (2005) Membrane-protein interactions in cell signaling and membrane trafficking. *Annu. Rev. Biophys. Biomol. Struct.* **34,** 119–151
34. Chien, A. J., and Hosey, M. M. (1998) Post-translational modifications of β-subunits of voltage-dependent calcium channels. *J. Bioenerg. Biomembr.* **30,** 377–386
35. Martin, S. W., Butcher, A. J., Berrow, N. S., Richards, M. W., Paddon, R. E., Turner, D. J., Dolphin, A. C., Sihra, T. S., and Fitzgerald, E. M. (2006) Phosphorylation sites on calcium channel α1- and β-subunits regulate ERK-dependent modulation of neuronal N-type calcium channels. *Cell Calcium* **39,** 275–292
36. Blom, N., Gammeltoft, S., and Brunak, S. (1999) Sequence and structure-based prediction of eukaryotic protein phosphorylation sites. *J. Mol. Biol.* **294,** 1351–1362
37. Rost, B., and Sander, C. (1993) Prediction of protein secondary structure at better than 70% accuracy. *J. Mol. Biol.* **232,** 584–599